ENHANCED ACTIVITY AND REUSABILITY OF TiO_2 LOADED MAGNETIC ACTIVATED CARBON FOR SOLAR PHOTOCATALYTIC OZONATION

Diego H. Quiñones[1], Ana Rey*[1], Pedro M. Álvarez[1], Fernando J. Beltrán[1], Pawel K. Plucinski[2]

[1]*Dpto. Ingeniería Química y Química Física, Universidad de Extremadura, Avda. Elvas s/n 06006 Badajoz (Spain)*

[2]*Department of Chemical Engineering. University of Bath. BA2 7AY. Bath. United Kingdom*

Abstract

Magnetically separable photocatalysts with high activity under solar illumination were successfully synthesized from a commercial meso-to-microporous activated carbon. First magnetite and then titania (anatase) were deposited onto the activated carbon support by impregnation and sol-gel methods, respectively. Various catalyst samples were prepared with different iron and titania contents. The synthesized photocatalysts were characterized by nitrogen adsorption, XRD, SEM, EDX, XPS and SQUID magnetometer. Photocatalytic performance of some selected samples was examined under various irradiation conditions in the wavelength ranges of 300-800 nm, 320-800 nm and 390-800 nm. Metoprolol tartrate (MTP) in aqueous solution (50 mg L^{-1}) was chosen as target compound for catalytic activity tests. The most efficient catalyst had TiO_2 and Fe mass compositions of 64 wt% and 9 wt%, respectively. It showed high activity in photocatalytic ozonation with complete removal of MTP in less than 2 h reaction time and 85% mineralization after 5 h. This catalyst was also easily separable due to its developed magnetic properties. Catalyst reusability and stability was proved to be rather good after completing a series of ten consecutive photocatalytic ozonation runs.

Keywords

Photocatalytic ozonation, magnetic photocatalyst, titania, metoprolol, water treatment, reusability.

1. Introduction

Given the global concern generated by the increasingly occurrence of emerging contaminants (ECs) in wastewater and aquatic environments, the research and development of novel water treatment technologies that can remove these compounds in a cost-efficient way is challenging.

Advanced oxidation processes (AOPs) involve the formation of highly reactive species, such as hydroxyl radical (·OH, E°=2.8V), which is capable of oxidizing most of the organic compounds in water [1]. Thus, various AOPs have demonstrated their ability to degrade many ECs transforming them into harmless products [2]. Among these AOPs, solar photocatalytic oxidation using TiO_2 as catalyst is one of the most promising cost-effective alternatives since it is a method capable of completely degrade organic ECs up to CO_2 and H_2O and also perform oxidative transformation of some inorganic compounds and deactivation of pathogenic microorganisms [3,4]. Recently, it has been shown that the combination of TiO_2 and ozone under sunlight illumination (i.e., solar photocatalytic ozonation) can greatly enhance the ECs degradation rates achieved by the single processes (i.e., ozonation and solar photocatalytic oxidation). The reason for such behavior is likely due to the adsorption of ozone onto the TiO_2 surface where it traps electrons promoted to the conduction band of the semiconductor, thus avoiding, to some extent, ineffective electron-hole recombination and generating ozonide radicals ($\cdot O_3^-$), which can be further transformed into hydroxyl radicals [5,6,7].

A key factor in the development of solar photocatalytic ozonation processes for the removal of ECs from water is the use of a suitable photocatalyst. In a previous work, a TiO_2 (anatase)-magnetic carbon composite (TiFeC) was synthesized and used for the degradation of metoprolol tartrate (MTP) [8]. MTP is a β-blocker pharmaceutical compound frequently found in effluents from sewage treatment plants [9,10]. After the treatment, the catalyst particles could be separated from the solution by an external magnet due to their superparamagnetic behavior, though their saturation magnetization was rather low (1.6 emu g^{-1}) compared to bulk magnetite (92 emu g^{-1}). Photocatalytic activity was fairly good though somewhat lower than that found for the commercially available catalyst AEROXIDE® TiO_2 P25. As part of our ongoing work on photocatalytic ozonation, this paper is focused on the optimization of TiFeC catalysts to improve their photocatalytic activity, separability and reusability. Also, this paper gives some insights into the elucidation of the mechanism of solar photocatalytic oxidation.

2. Experimental section

2.1. Catalysts preparation

Samples of magnetic photocatalysts were prepared following a method described previously, which comprises three main steps [11]. The first step was the synthesis of magnetic activated carbon particles (FeC) following the incipient wetness impregnation method reported by Fuentes and Tartaj [12]. Typically, 10 g of granular activated carbon (Darco 12-20, Sigma–Aldrich) were impregnated with an iron (III) nitrate ethanol solution. In order to have samples with different final iron content (10-30 wt% Fe), solutions of different concentrations (920-1190 g L^{-1}) were used. Impregnated samples were dried at 90ºC for 2 h and then 150 mmol of ethylene glycol was added to reduce Fe^{3+} to Fe^{2+}. Finally, the samples were subjected to heat treatment under nitrogen atmosphere at 350-550ºC for 2-4 h. The particles thus obtained were milled and sieved so that only particles with size lower than 125 μm were selected. The second stage was the synthesis of a TiO_2 nanosol. To prepare 1 g of TiO_2, 4.3 mL of titanium (IV) butoxide (97%, Aldrich) were diluted in 1.4 mL of isopropanol (>99%, Aldrich) and the mixture was added dropwise to 34 mL of distilled water acidified at pH 2.0 with HNO_3 (65%, Panreac). The solution was stirred under reflux at 75°C for 24 h. Finally, the excess of alcohol was removed on a rotary evaporator operating at 80°C under vacuum, thus obtaining a TiO_2 nanosol. The final stage of the catalyst preparation was the dispersion of FeC particles in the TiO_2 nanosol under sonication for 1 h. Subsequently, the dispersion was dried under vacuum at 80°C. The residue was repeatedly washed with distilled water until no total organic carbon (TOC) was detected in the supernatant. After each washing step the particles were separated from the liquid phase by an external magnet so that the non-magnetic particles were discarded. Finally, the particles were dried at 100°C overnight and kept in a desiccator until further use in photocatalytic tests. Table 1 shows the amounts of activated carbon (AC), Fe, FeC support and Ti and calcination conditions (step 1) used in the preparation of three magnetic catalysts selected for photocatalytic experiments.

TABLE 1

2.2. Characterization of the catalysts

The characterization of the catalysts was carried out by N_2 adsorption-desorption, X-ray diffraction (XRD), scanning electron microscopy (SEM-EDX), X-ray photoelectron spectroscopy (XPS), inductively coupled plasma mass spectrometry (ICP-MS) and SQUID magnetometry.

BET surface area and pore structure of the AC used as support and the prepared photocatalysts were determined from their nitrogen adsorption–desorption isotherms obtained at -196ºC using an Autosorb 1 apparatus (Quantachrome). Prior to analysis the samples were outgassed at 250°C for 12 h under high vacuum (<10^{-4} Pa). The *t*-plot method was applied to obtain external surface area and micropore volume of samples.

The crystalline phases present in the catalysts and AC were inferred from their X-ray diffraction (XRD) patterns recorded using a Bruker D8 Advance XRD diffractometer with a CuKα radiation (λ = 0.1541 nm). The data were collected from 2θ = 20° to 70° at a scan rate of 0.02 s^{-1} and 1 s per point.

The particle morphology of the catalysts was analyzed using a Hitachi S-4800 scanning electron microscope with 20–30 kV accelerating voltage and 500–2000 magnification. Catalysts were also examined by energy dispersive X-ray (EDX) in order to determine the distribution of Ti and Fe on the particles using a SSD detector XFlash 5010 (Bruker), with 5 kV accelerating voltage and 500–2000 magnification.

XPS spectra were obtained with a Kα Thermo Scientific apparatus with an Al Kα ($h\nu$=1486.68 eV) X-ray source using a voltage of 12 kV under vacuum ($2x10^{-7}$ mbar). Binding energies were calibrated relative to the C1s peak from carbon samples at 284.6 eV. The resulting XPS peaks were curve-fitted to a combination of Gaussian and Lorentzian functions using a Shirley type background for peak analysis.

The iron content of the catalysts was analyzed by inductively coupled plasma with an ICP-MS NexION 300D (Perkin-Elmer) after acidic microwave digestion of the samples. The content of TiO_2 was estimated from the residue of catalyst combustion in air at 900°C, taking into account the amount of iron and the ash content on the AC support used.

Magnetic properties of the materials were tested by magnetometry using a Quantum Design MPMS XL-7 Superconducting Quantum Interference Device (SQUID). The magnetic moment *M* was measured as function of the applied magnetic field *H* at room temperature.

2.3. Photocatalytic activity measurements

Metoprolol tartrate (>99% Sigma) (MTP) was used as target contaminant to test the catalytic activity of the synthesized materials in photocatalytic oxidation, photocatalytic ozonation, and catalytic ozonation experiments. In addition, experiments of adsorption of MTP onto AC and MTP ozonation, both in the darkness and under illumination (i.e., photolytic ozonation), were completed.

Photocatalytic experiments were carried out in semi-batch mode in a laboratory-scale system consisting of a 1 L glass-made cylindrical reactor with an internal diameter of 10.7 cm, provided with a gas inlet, a gas outlet and a liquid sampling port. The reactor was placed in the chamber of a commercial solar simulator (Suntest CPS, Atlas) provided with a 1500 W air-cooled Xe arc lamp with emission restricted to wavelengths over 300 nm because of the presence of quartz and glass cut-off filters. The irradiation intensity was kept at 550 W m^{-2} and the temperature of the system was maintained between 25 and 40°C throughout the experiments. If required, a laboratory ozone generator (Anseros Ozomat Com AD-02) was used to produce a gaseous ozone-oxygen stream that was fed to the reactor. In that case, the ozone concentration was recorded on an Anseros Ozomat GM-6000Pro gas analyzer.

In a typical photocatalytic ozonation experiment, the reactor was first loaded with 750 mL of an aqueous solution containing 50 mg L^{-1} MTP initial concentration. Then, 0.28 g of the catalyst were added and the suspension was stirred in the darkness for 30 min while bubbling air to the system. After this dark stage, the lamp was switched on and, simultaneously, a mixture of ozone-oxygen (6 mg L^{-1} ozone concentration) was fed to the reactor at a flow rate of 20 L h^{-1}. The irradiation time for each experiment was 5 h. Samples were withdrawn from the reactor at intervals and filtered through a 0.2 μm PET membrane to remove the photocatalyst particles.

MTP adsorption (i.e., absence of radiation and ozone), MTP single ozonation (i.e., absence of radiation and catalyst), MTP catalytic ozonation (i.e., absence of radiation) and MTP photolytic ozonation (i.e., absence of catalyst) experiments were also carried out for comparative analysis. In addition, the ability of radiation to decompose ozone in the absence of MTP was tested. For that, the photoreactor was loaded with 750 mL of ozone saturated-ultrapure water (C_{O30}~$1.6x10^{-4}$ M) and the system was allowed to react either under illumination or in the dark for 10 min.

Some experiments were carried out supplementing the reaction device with specific filter sheets that selectively block UV radiation. To cut off all the wavelengths below 390 nm, a flexible polyester thin film (Edmund Optics) was used while a polyester film (Unipapel) was used to cut off UV radiation below 320 nm.

To test the reusability of a selected catalyst, ten consecutive photocatalytic ozonation experiments were carried out recovering the catalyst particles with an external magnet after each experiment and reusing them in the next run.

MTP concentration was analyzed by high-performance liquid chromatography (Hitachi, Elite LaChrom) using a Phenomenex C-18 column (5 μm, 150 mm long, 3 mm diameter) as stationary phase and 0.5 mL min^{-1} of 15:85 acetonitrile:acidified water (0.1% phosphoric acid) as mobile phase (isocratic). An UV detector set at 225 nm was used for detection. Total organic

carbon (TOC) was measured using a Shimadzu TOC-V_{SCH} analyzer. Aqueous ozone was measured by following the indigo method using a UV-Visible spectrophotometer (Evolution 201, Thermospectronic) set at 600 nm [13]. Ozone in the gas phase was continuously monitored by means of an Anseros Ozomat GM-6000Pro analyzer. Hydrogen peroxide concentration was determined photometrically by the cobalt/bicarbonate method, at 260 nm using a UV-Visible spectrophotometer (Evolution 201, Thermospectronic) [14]. Iron and titanium in solution were analyzed by inductively coupled plasma mass spectrometry using a Perkin Elmer NexION 300D ICP-MS apparatus.

3. Results and discussion

3.1. Characterization of the fresh catalysts

Table 2 summarizes the composition, crystallite sizes and main textural parameters of three selected TiFeC catalysts and the starting AC. Also, properties of a catalyst after being used in ten consecutive photocatalytic ozonation runs (namely TiFeC-3*) are shown in Table 2.

TABLE 2

As it can be seen in **Table 2**, catalyst TiFeC-1 had lower Fe and TiO_2 contents than the catalysts TiFeC-2 and TiFeC-3 as a result of a lower metal loading during the preparation method (see **Table 1**). The catalysts TiFeC-2 and TiFeC-3 had a similar content of TiO_2 and C but the amount of Fe in the latter was almost 20% higher than in the first. This suggests that calcination conditions (see **Table 1**) play an important role in the fixation of Fe to the carbon surface. Regarding TiO_2 mass composition of the TiFeC catalysts, the final titania content of the catalysts was always somewhat lower than expected (i.e. 66 wt.% for TiFeC-1 and 80 wt.% for TiFeC-2 and TiFeC-3) likely due to the loss of some TiO_2 during the washing steps of the synthesis procedure.

Fig. 1 shows the XRD patterns obtained for the AC support and TiFeC catalysts. From the AC diffractogram, some characteristic diffraction peaks of graphite can be identified, as the two broad peaks at 2θ = 26 and 43º. Other diffraction peaks are due to the presence of SiO_2–quartz and SiO_2–cristoballite particles which are common minerals in the activated carbon used in this work [8]. Regarding the TiO_2 structure, XDR patterns obtained for the three catalysts show diffraction peaks at 25.4, 37.9, 47.9, 54.4 and 62.8° which confirm the presence of anatase in all cases. The anatase crystallite size, d_A, was calculated from the (101) diffraction peak using the Scherrer equation and the results are summarized in **Table 2**. It can be noticed a slight increase in the anatase particle size with the increasing content of TiO_2 on the catalyst. Fe_3O_4 magnetite

or γ-Fe_2O_3 maghemite species could also be identified (these two are indistinguishable by XRD) in the XRD patterns of the TiFeC catalysts with main reflection peaks at 30.2, 35.6, 43.1 and 57.0º. The intensity of the main peaks increases according to the sequence TiFeC-1<TiFeC-2<TiFeC-3, which is likely connected to the higher amount of iron loaded on the last two samples and the more drastic heat treatment carried out for their preparation. The magnetite-maghemite crystallite sizes were calculated by means of the Scherrer equation from the (311) diffraction peak. As can be seen in Table 2, the catalysts TiFeC-2 and TiFeC-3 exhibited a much larger crystallite size than the catalyst TiFeC-1.

FIGURE 1

BET area, $S_{BET,}$ external surface area, S_{ext}, and micropore volume, $V_{MICRO,}$ were obtained from the nitrogen adsorption–desorption isotherms (not shown) and their values are presented in **Table 2**. All the samples showed type I isotherm, as it has already been reported for this type of samples [8], which is characteristic of microporous materials. The micropore volume of the prepared catalysts was much lower than that of the starting AC, which suggests that iron oxides and TiO_2 might block some pore entrances of the AC [11]. On the other hand, the external surface areas of the catalysts were larger than that of the AC. This can be due to the generation of agglomerates of TiO_2 on the surface of the AC, thus giving rise to the formation of new larger pores in the range of meso and macropores.

Fig. 2 shows SEM images of the three catalysts and the distribution of Fe and Ti species by means of energy dispersive X-ray analysis (EDX). As can be seen in the images, the particle size distribution is wide with particles in the 5-125 μm size range. A non-uniform distribution of Fe and Ti on all the three catalysts could be observed (see **Fig.2**, right). However, it is important to note that Fe can be found in all the particles analyzed since catalyst particles were magnetically separated after the washing steps in the catalyst preparation method.

FIGURE 2

Surface chemical composition of the catalysts was analyzed by XPS and the results are summarized in **Table 3** and **Fig. 3** (only for catalyst TiFeC-3 as an example). XPS full spectra of the three catalysts confirmed the presence of C, Ti, O and Fe on their surface (see **Fig. 3(a)** for catalyst TiFeC-3). The surface composition of the catalysts (**Table 3**) was calculated from peak areas and Wagner atomic sensitivity factors [15]. It can be noticed that all the catalyst presented fairly similar atomic surface Ti content though somewhat lower in catalyst TiFeC-2. On the other

hand, the percentage of atomic surface Fe increased as bulk iron content of the catalysts was larger (see also **Table 2**), being the highest on the catalyst TiFeC-3.

TABLE 3

Fig. 3(b) shows the high-resolution Ti 2p XPS spectrum for catalyst TiFeC-3. The binding energy peaks located at 459.8 and 465.5 eV can be attributed to the spin-orbit splitting of the Ti 2p components (Ti $2p_{3/2}$ and Ti $2p_{1/2}$), with a difference in binding energy of ca. 5.7eV, which confirms the presence of Ti as Ti^{4+} (TiO_2) [16,17]. Similarly, **Fig. 3(c)** displays the high resolution Fe 2p XPS spectrum for catalyst TiFeC-3. The peak positions of Fe $2p_{3/2}$ and Fe $2p_{1/2}$ at ca. 710.7 and 724.8 eV, respectively, are consistent with the existence of magnetite (Fe_3O_4) [18,19]. On the other hand, the presence of satellite peaks at ca. 718.9 and 715.4 eV is attributable to the existence of Fe^{3+} and Fe^{2+} iron species, respectively [18]. Since it has been previously reported that Fe $2p_{3/2}$ for pure Fe_3O_4 does not have a satellite peak [20], the coexistence of other iron species such as maghemite (γFe_2O_3) or FeO cannot be disregarded. Similar XPS results were found for the three fresh catalysts, as can be inferred from data in Table 3.

FIGURE 3

Due to the presence of magnetic iron species (magnetite and/or maghemite) in the catalysts, magnetization of the samples was analyzed and results are depicted in **Fig. 4**. As expected, higher iron content led to higher saturation magnetization (M_s) of the samples (see value for M_s in **Fig. 4**). The catalyst TiFeC-3, which was synthesized under the most drastic conditions in terms of temperature and time of the heat treatment and also had the highest iron content among the prepared catalysts (see **Table 1**), is the one that presented the highest M_s. For this catalyst, the value of saturation magnetization was found to be 4.4 emu g^{-1}. Taking into account the iron content of this sample and considering that all iron could be converted into magnetite (bulk magnetite 92 emu g^{-1}) a maximum M_s of 12 emu g^{-1} could be expected. However, it should be pointed out that magnetization of magnetite depends on the particle size and the particle distribution. Thus, M_s values lower than that of bulk magnetite (in the 60-70 emu g^{-1} range) have been found for magnetite particles of similar sizes of the crystallites found in TiFeC catalysts (~10-20 nm) [21]. Also, magnetite readily reacts with oxygen to form maghemite, which has lower M_s than magnetite. Accordingly, partial oxidation of magnetite to maghemite in TiFeC catalysts is likely to take place. TiFeC-3 presented a much higher M_s value than TiFeC-1 and TiFeC-2, which could suggests a higher content of magnetic iron oxide (magnetite and maghemite) as also deduced from XRD and XPS results. This means that not only the iron

content but also the heat treatment conditions (temperature and time) influences on the final content of magnetic iron oxide. It is also important to note that all the TiFeC catalysts showed zero coercitivity and remanent magnetization indicating superparamagnetic behavior and thus the particles could be re-dispersed in solution for reuse after being separated by a magnet.

FIGURE 4

3.2. Catalytic activity

The photoactivity of the synthetized catalysts was evaluated through simulated solar-light radiation (300-800 nm) photocatalytic oxidation and photocatalytic ozonation experiments aimed to degrade MTP. Some additional experiments were carried out to analyze the contributions of adsorption, direct ozonation and catalytic ozonation to the removal of MTP during the photocatalytic ozonation process. An initial concentration of MTP as high as 50 mg L^{-1} was used in the experiments, which allows us to analyze the effect of the catalysts in terms of mineralization (i.e. TOC depletion). **Fig. 5** shows the time evolution of MTP concentration and TOC during the course of some selected experiments.

FIGURE 5

As shown, MTP was adsorbed onto any of the catalysts surface to some extent, being the catalyst TiFeC-1 which presented the highest adsorption capacity (18% MTP removed after 5 h) while MTP uptake on catalysts TiFeC-2 and TiFeC-3 was only c.a. 12%. This result is in agreement with the highest BET surface area of TiFeC-1 (see **Table 2**). It can be also noticed that in all cases adsorption equilibrium was practically reached in about 30 min, so relatively fast MTP adsorption took place.

Regarding photocatalytic oxidation, catalysts TiFeC-2 and TiFeC-3 were shown to be more efficient to degrade MTP than TiFeC-1 as it can be noticed in **Fig. 5**. As seen in **Fig. 5**, final MTP conversions obtained with catalysts TiFeC-2 and TiFeC-3 were ca. 60% while only 45% MTP conversion was reached when using the catalysts TiFeC-1. From these results, and taking into account the difference found in the TiO_2 content of the catalysts (TiFeC-2 and TiFeC-3 had a 10% more TiO_2 than TiFeC-1, see **Table 2**), the removal efficiency of MTP may be mainly due to the oxidizing species generated by the photo-excitation of titania particles loaded onto the catalysts rather than to the adsorption capacity of the materials. Contribution of direct photolysis to the removal of MTP can also be ruled out as MTP does not absorb radiation at wavelength higher than 300 nm. From XPS results quite similar surface atomic Ti amounts were present on the three catalysts (**Table 3**), accordingly it can be suggested that the simulated solar radiation

could penetrate more than a few nanometers in samples (depth of XPS analysis), thus exciting TiO_2 particles located at deeper sites on the activated carbon. Contrary to MTP removal, TOC removal after 5 h was higher when using catalyst TiFeC-1 (c.a. 30% conversion) than in experiments using TiFeC-2 and TiFeC-3 (c.a. 20% conversion). This suggests that catalyst TiFeC-1 is able to absorb MTP degradation products to a higher extent than TiFeC-2 or TiFeC-3.

As can be observed in **Fig. 5**, all the treatments using ozone (i.e. single ozonation, catalytic ozonation, photolytic ozonation and photocatalytic ozonation) led to much faster MTP degradation rates than the photocatalytic oxidation treatment regardless of the catalyst used. In all ozonation experiments MTP depletion rate was quite similar, which suggests that MTP removal occurs mainly through direct ozone reaction with low catalytic effect. Similar results have been observed previously for compounds that react fast with ozone, such as diclofenac and sulfamethoxazole [22]. MTP has also a relatively high rate constant for its reaction with ozone (k_{O3} = 2.9×10^2 M^{-1} s^{-1} at pH 6) [23]. Main differences among ozone processes were observed in mineralization profiles.

Single ozonation led to just about 40% TOC removal after the 5-hour reaction period. Ozone, despite being a strong oxidizing agent, reacts selectively primarily with aromatic and unsaturated compounds. As a result of direct ozonation of MTP non-aromatic and non-unsaturated intermediates compounds are formed (e.g., short-chain carboxylic acids), which react slowly with ozone. As a result, they are accumulated in water [24,25].

The presence of catalyst greatly improved mineralization rates compared to ozone alone. Thus, TOC conversion reached 40-50% and 70-90% after catalytic ozonation and photocatalytic ozonation experiments, respectively. Various catalytic and photolytic effects leading to the formation of hydroxyl radicals, which can unselectively oxidize organic compounds in water, can be addressed. First, in the absence of radiation (i.e., catalytic ozonation), ozone can be partially transformed into hydroxyl radicals by the action of the activated carbon used as support [26,27,28,29] as well as the supported TiO_2 [29,30] and iron oxides [29,31]. According to the results shown in **Fig.5** it is apparent that the effects of metal oxides (TiO_2 and or iron oxides) were greater than that of the AC, as higher TOC conversions were achieved with catalyst TiFeC-2 and TiFeC-3, which had higher amounts of Ti and Fe in their composition than catalyst TiFeC-1. In the presence of radiation (i.e., photocatalytic ozonation), in addition to the aforementioned catalytic effects, ozone can absorb UV-photons to yield excited atomic oxygen species that further generate hydroxyl radicals [32,33]. Thus, as can be seen in **Fig. 5**, 65%

TOC conversion was reached in the photolytic ozonation experiment in contrast to 40% achieved in the single ozonation experiment carried out in the absence of radiation. In addition, the well-know photocatalytic effect of the semiconductor anatase must be considered. This effect can be greatly improved by the presence of ozone, which due to its electrophilic nature, is prone to trap the electrons from the semiconductor conduction band generating ozonide radicals, which are further transformed into additional $^{\bullet}OH$ [5,6]. Finally, iron oxides present in the catalysts could also play a photocatalytic role. Thus, as hydrogen peroxide can be generated from ozonation of MTP [24], iron oxides can catalyze photo-Fenton like reactions.

3.2.1. Effect of radiation wavelength

The results above show the importance of photolytic decomposition of ozone in the MTP mineralization rate. To evaluate the effect of the radiation wavelength in the photolytic ozonation process, some experiments were carried out using filters that selectively cut off particular wavelengths from the solar spectrum. **Fig. 6** shows the evolution of MTP concentration and TOC with time during photolytic ozonation experiments carried out with radiation of wavelengths ranging between 300-800, 320-800 and 390-800 nm. Results from a single ozonation experiment in the darkness are also shown.

FIGURE 6

As shown in **Fig. 6**, MTP removal profiles were quite similar for all the experiments suggesting that MTP was mainly removed through direct reaction with ozone and the effect of radiation was negligible. However, from TOC results, it is evident that the 300-320 nm radiation enhanced the efficiency of TOC removal due to photolytic transformation of ozone into reactive oxygen species, which would eventually be transformed into in hydroxyl radicals [33].

To quantify the effect of different radiation wavelengths on the ozone decomposition, some experiments of ozone photolytic depletion from ozone saturated-ultrapure water were carried out. Aqueous ozone decomposition followed pseudo-first order kinetics:

$$-\frac{dC_{O3}}{dt} = k_{app} \cdot C_{O3} \quad (1)$$

Fitting results of experimental data to eq. (1), the values summarized in **Table 4** for the apparent rate constant were obtained. Since no great differences were found for the apparent rate constant in the darkness and under illumination with 320-800 and 390-800 nm radiation while k_{app} was much higher for the process under illumination with 300-800 nm radiation, it could be

confirmed that the photolytic decomposition of ozone occurs primarily at wavelengths from 300 to 320 nm. Radiation wavelength over 320 nm does not significantly produce ozone photolysis and, therefore, did not improve MTP mineralization process performance.

TABLE 4

Fig. 7 shows the TOC profiles during some photocatalytic ozonation experiments carried out with different wavelength radiation and using TiFeC catalysts. Results from photolytic experiments (in the absence of catalyst) are also shown.

FIGURE 7

As a general trend, from Fig. 7 it can be noticed that regardless of the radiation wavelength, the presence of any of the catalyst increased to some extent the MTP mineralization rate. When irradiated with 390-800 nm radiation (Fig. 7 (c)), the three catalysts led to similar mineralization degree. When compared with the results obtained in a catalytic ozonation experiment (Fig. 5), only slightly higher mineralization percentages were reached in the presence of the irradiated catalysts, suggesting that they have low activity under visible light irradiation.

Photocatalytic ozonation systems mediated by 300-800 and 320-800 nm radiation led to similar mineralization percentages with somewhat higher mineralization rate by using 300-800 nm radiation. These results are in contrast to photolytic ozonation that lost efficiency at 320-800 nm since the production of hydroxyl radicals from ozone photodissociation is minimized at wavelengths higher than 320 nm. Thus, when using 300-800 nm radiation, the catalytic effect of the synthetized materials can be masked by the ozone photolysis reaction, being preferable to use radiation of wavelength higher than 320 nm to evaluate the catalytic activity in the process studied (photocatalytic ozonation). In that sense, Fig. 7 (b) shows that higher mineralization rates were obtained in the presence of the catalysts being TiFeC-2 and TiFeC-3 the catalysts with the best performance.

3.2.2. Simplified mechanistic approach

According to the above results, the reaction mechanism that takes place in the overall MTP photocatalytic ozonation process with a TiFeC catalyst could be explained as the sums of contributions and synergy of several processes (i.e. direct ozone reaction, ozone photolytic decomposition, heterogeneous photocatalysis, Fenton and photo-Fenton reactions, etc.). Fig. 8 shows the time-evolution of dissolved ozone and hydrogen peroxide during single ozonation,

catalytic ozonation and photocatalytic ozonation experiments carried out in the presence of catalyst TiFeC-3.

FIGURE 8

From **Fig. 8** (left) it can be noticed that ozone accumulated in solution during the single ozonation experiment reaching its maximum concentration at about 30 min reaction time, then slowly decreasing its concentration with time. A similar profile was observed during catalytic ozonation but with a slightly faster depletion rate. In contrast, in photocatalytic ozonation reaction, the maximum concentration of dissolved ozone was noticeably lower and a faster depletion rate was observed during the first 60 min, leading to a nearly steady concentration of about $5x10^{-6}$ M. The lowest values of dissolved ozone and the highest mineralization rate observed in the photocatalytic ozonation experiment suggest that besides direct MTP-O_3 reaction, or in lesser extent side reactions with catalyst surface (activated carbon or iron), O_3 was also consumed through its reaction with electrons on the TiO_2 surface improving MTP mineralization due to the generation of additional hydroxyl radicals [6,34].

Generation of hydrogen peroxide by direct ozonation of MTP has been previously proposed as a step of MTP degradation mechanism [35]. This has been confirmed experimentally in this work, as shown in **Fig. 8** (right). In contrast, H_2O_2 concentration during the photocatalytic ozonation experiment was much lower likely due to the consumption of H_2O_2 through surface photo-Fenton reactions (liquid bulk photo-Fenton reactions could be neglected as the concentration of iron in solution was rather low ca. $1.5x10^{-7}$ M) and/or its reaction on the TiO_2 surface as electron acceptor.

According to the findings of this work, it can be postulated that photocatalytic ozonation of MTP with TiFeC catalysts takes place through reactions (2) to (11), where ozone is the main species responsible for MTP disappearance and ·OH (on the catalyst surface or in solution) is the main responsible species for MTP mineralization.

MTP direct ozonation:

$$MTP + O_3 \longrightarrow I + H_2O_2 \quad (2)$$

where *I* represents any intermediate by-product of MTP oxidation pathway.

Hydroxyl radical attack to intermediate products:

$$I + {}^{\bullet}OH \longrightarrow CO_2 + H_2O \quad (3)$$

Hydroxyl radical formation:

$$O_3 + CAT_{AC,Fe} \longrightarrow [...] \longrightarrow {}^{\bullet}OH \quad (4)$$

$$H_2O_2 + CAT_{Fe} \longrightarrow [...] \longrightarrow {}^{\bullet}OH \quad (5)$$

$$O_2 + CAT_{TiO_2} + h\nu_{300-390\,nm} \longrightarrow [...] \longrightarrow {}^{\bullet}OH \quad (6)$$

$$O_3 + h\nu_{300-320\,nm} \longrightarrow [...] \longrightarrow {}^{\bullet}OH \quad (7)$$

$$O_3 + CAT_{TiO_2} + h\nu_{300-390\,nm} \longrightarrow [...] \longrightarrow {}^{\bullet}OH \quad (8)$$

$$H_2O_2 + CAT_{Fe,TiO_2} + h\nu_{300-390\,nm} \longrightarrow [...] \longrightarrow {}^{\bullet}OH \quad (9)$$

$$H_2O_2 \xleftrightarrow{pK=11.3} H^+ + HO_2^- \quad (10)$$

$$O_3 + HO_2^- \longrightarrow [...] \longrightarrow {}^{\bullet}OH \quad (11)$$

Reactions (4) to (9) and (11) involve intermediate steps that have been represented as […]. Reaction (4) also involves the catalytic effect of activated carbon and iron in the catalyst in the ozone decomposition reaction; reaction (5) would be mainly due to Fenton like reaction due to the iron species in the catalyst surface; reaction (6) represents the conventional photocatalytic oxidation (with oxygen) set of reactions; (7) is the photolytic decomposition of ozone that has been proved to take place at wavelengths between 300-320 nm; reaction (8) involves the role of ozone as electron acceptor on the TiO_2 surface; reaction (9) considers, as a whole, the photo-Fenton reactions on the catalyst surface and the role of hydrogen peroxide as electron acceptor on the TiO_2 surface; and reaction (11) groups the series of reactions that yield hydroxyl radical from the starting reaction between ozone and hydroperoxide ion.

The relative contribution of each step to the overall process would depend on the experimental reaction conditions (e.g., pH, ozone dose, radiation wavelength) and the catalyst structure and composition. This issue will be the subject of a future work.

3.3. Catalyst reusability

Since catalyst TiFeC-3 showed the best catalytic performance and separability, further experiments were carried out to test its stability and reusability. Thus, a series of ten

consecutive MTP photocatalytic ozonation runs were performed under 320-800 nm radiation. This wavelength range was chosen to isolate to some extent the catalytic effect. Thus, at those conditions the effect of the photocatalytic route on the MTP mineralization is high while keeping low the contribution of the photolysis of ozone.

Fig. 9 shows TOC removal percentages obtained after the ten consecutive runs (5 h each) reusing the catalyst. After each run the catalyst was easily separated from the liquid by means of a magnet placed outside at the bottom of the reactor. After removing the liquid, a new fresh MTP solution was added to the reactor to start the following run.

FIGURE 9

As shown in **Fig. 9** the catalyst exhibited no significant catalytic loss keeping overall TOC removal at about 75-80% decrease surmounting 80% mineralization during the first 6 runs and 75% mineralization for the last 4 runs. It is important to note here that in all runs complete removal of MTP was achieved in less than 2 hours. Also, no significant changes were observed throughout the series of runs in the value of the apparent pseudo-first order rate constant calculated for MTP depletion (see **Table 5**). Table 5 also shows the concentration of iron found in solution after each run. As can be observed very low amount of iron was leached from the catalyst being the aqueous concentration always lower than 0.1 mg L^{-1}. From the mass balance, the total amount of iron leached out of the catalyst after the ten runs was found to be only a 0.25% of the amount initially present. Regarding titanium, after each run its concentration was lower than 10 μg L^{-1}.

TABLE 5

Therefore, the catalyst TiFeC-3 seems to be very stable and easily separable to be used in repeated runs or even in continuous flow experiments. However, the reaction medium (ozone, hydroxyl radicals, radiation, etc.) could provoke the modification of some important properties of the catalysts apart from iron or titanium leaching. In this line, the catalyst recovered after being used in the ten consecutive runs (named as TiFeC-3* in tables and figures) was characterized.

Form the XRD patterns (**Fig. 1**) no significant changes were observed when comparing the fresh and used catalysts. Anatase and magnetite/maghemite patterns could be identified in both diffractograms and no substantial changes in the crystallite sizes were observed (**Table 2**). Also in **Table 2**, textural properties of the fresh and used catalysts are summarized. All the textural parameters underwent a slight decrease after using the catalyst for 50 h, although these lower values seem not to affect the catalytic activity of the material. Also SEM and EDX images (**Fig.**

2) show no apparent modification on the catalyst surface where a non-uniform distribution of iron and titanium is observed. On the other hand, XPS results are summarized in **Table 3**. It can be noticed a slight decrease in the surface carbon content of the used sample respect to the fresh one and an increase in the surface iron content (from 3.4 to 5.1%). This can be due to the reaction between ozone and carbon atoms in the surface of AC, that can release organic products to the liquid reaction medium leading to a catalyst mass loss [36], and leaving more iron exposed on the catalyst surface. Regarding to the surface species on the catalysts, no significant differences were found in the XPS spectra of C 1s, O 1s and Ti 2p. However, iron Fe 2p XPS spectra showed slight differences and it has been plotted in **Fig. 3** for comparison purposes. First of all, it can be observed that the Fe $2p_{1/2}$ and Fe $2p_{3/2}$ peaks are wider in the used catalyst and have been shifted to higher binding energies likely due to the partial oxidation of the surface iron species from Fe^{2+} to Fe^{3+}, which is also confirmed by de absence of Fe^{2+}-satellite peak [20]. This is in a good agreement with the results observed in the magnetization of the sample (**Fig. 4**) where the used catalysts presented a slightly lower saturation magnetization (4.1 vs. 4.4 emu g^{-1}) likely due to the partial oxidation of surface magnetite.

Therefore, main changes produced in the catalyst surface after used are related to the partial oxidation of carbon and surface iron species, which reduced its saturation magnetization to a relatively low extent (around 7%). However, the catalyst still presented a fairly high saturation magnetization and could be easily recovered from the reaction medium by an external magnet and also kept high catalytic activity.

4. Conclusions

The TiO_2-anatase loaded magnetic activated carbon catalysts synthesized in this work showed good photocatalytic activity and separability. Optimization of iron content and heat treatment conditions within the synthesis of the magnetic activated carbon support are crucial to obtain an easily magnetically separable catalyst. TiFeC catalyst led to complete removal of MTP and high levels of mineralization (70-90%) in photocatalytic ozonation experiments with simulated solar light. MTP was mainly removed through direct ozone reaction independently of the catalyst composition. However, MTP mineralization (i.e., conversion up to CO_2) rate highly depends on the anatase content of the catalyst. Photocatalytic ozonation is a complex process involving a synergy of different reaction pathways (i.e. ozone direct reactions, ozone and hydrogen peroxide electron capture from TiO_2 surface, ozone photolysis with radiation wavelength between 300-320 nm, Fenton and photo-Fenton reactions and catalytic ozonation) leading to the degradation of organic pollutants in water (MTP in the case study).

Stability and reusability of a TiFeC catalyst was demonstrated to be rather good through a series of ten consecutive photocatalytic ozonation runs. After use, the properties of the catalyst did not vary significantly from the fresh sample though partial oxidation of carbon and surface iron species took place. However, the ten times reused catalyst could still be easily separated by an external magnetic field, which makes this type of catalysts an interesting alternative for solar photocatalytic processes.

Acknowledgements

This work has been supported by the Spanish Ministerio de Economía y Competitividad (MINECO) and European Feder Funds through the project CTQ2012-35789-C02-01. Authors acknowledge the SAIUEX service of the University of Extremadura for the characterization analyses. P.M. Álvarez thanks the Ministerio de Educación, Cultura y Deporte of Spain for providing a sabbatical grant (PR2011-0572). A. Rey thanks the University of Extremadura for a postdoctoral research grant. D.H. Quiñones thanks the MINECO for a predoctoral FPI grant.

References

[1] Andreozzi , V. Caprio, A. Insolab, R. Marotta. Advanced oxidation processes (AOP) for water purification and recovery. Catal. Today 53 (1999) 51–59.

[2] K. Ikehata, M. Gamal El-Din, S.A. Snyder. Ozonation and Advanced Oxidation Treatment of Emerging Organic Pollutants in Water and Wastewater. Ozone Sci. Eng. 30 (2008) 21–26.

[3] S. Malato, P. Fernández-Ibáñez, M.I. Maldonado, J. Blanco, W. Gernjak. Decontamination and disinfection of water by solar photocatalysis: Recent overview and trends. Catal. Today 147 (2009) 1-59.

[4] D.S. Bhatkhande, V.G. Pangarkar, A.A.C.M. Beenackers. Photocatalytic degradation for environmental applications – a review. J. Chem. Technol. Biotechnol. 77 (2001) 102-116.

[5] R. Rajeswari, S. Kanmani. TiO2-based heterogeneous photocatalytic treatment combined with ozonation for carbendazim degradation. J. Environ. Health Sci. Eng. 6 (2009) 61-66.

[6] T.E. Agustina, H.M. Ang, V.K. Vareek. A review of synergistic effect of photocatalysis and ozonation on wastewater treatment. J. Photochem. Photobiol. C Photochem. Rev. 6 (2005) 264-273.

[7] E.M. Rodríguez, G. Fernández, P.M. Alvarez, F.J. Beltrán. TiO_2 and Fe (III) photocatalytic ozonation processes of a mixture of emergent contaminants of water. Water Res. 46 (2012) 152-166.

[8] A. Rey, D.H. Quiñones, P.M. Álvarez, F.J. Beltrán, P.K. Plucinski. Simulated solar-light assisted photocatalytic ozonation of metoprolol over titania-coated magnetic activated carbon. Appl. Catal. B Environ. 111-112 (2012) 246-253.

[9] B. Kasprzyk-Hordern, R.M. Dinsdale, A.J. Guwy. The removal of pharmaceuticals, personal care products, endocrine disruptors and illicit drugs during wastewater treatment and its impact on the quality of receiving waters. Water Res. 43 (2009) 363-380.

[10] M.D. Hernando, M. Mezcua, A.R. Fernández-Alba, D. Barceló. Environmental risk assessment of pharmaceutical residues in wastewater effluents, surface waters and sediments. Talanta 69 (2006) 334-342.

[11] Y. Ao, J. Xu, D. Fu, C. Yuan. A simple route for the preparation of anatase titania-coated magnetic porous carbons with enhanced photocatalytic activity. Carbon 46 (2008) 596-603.

[12] A.B. Fuertes, P. Tartaj. A facile route for the preparation of superparamagnetic porous carbons. Chem. Mater. 18 (2006) 1675-1679.

[13] H. Bader, J. Hoigné. Determination of ozone in water by the indigo method. Water Res. 15 (1981) 449–456.

[14] W. Masschelein, M. Denis, R. Ledent. Spectrophotometric determination of residual hydrogen peroxide. Water Manag. Water Sewage Works, August (1977) 69-72.

[15] C.D. Wagner, L.E. Davis, M.V. Zeller, J.A. Taylor, R.H. Raymond, L.H. Gale. Empirical atomic sensitivity factors for quantitative analysis by electron spectroscopy for chemical analysis. Surf. Interf. Anal. 3 (1981) 211-225.

[16] P. Fu, Y. Luan, X. Dai. Preparation of activated carbon fibers supported TiO2 photocatalyst and evaluation of its photocatalytic reactivity. J. Mol. Catal. A Chem. 221 (2004) 81-88.

[17] Y. Zhang, P. Xiao, X. Zhou, D. Liu, B. Batalla, G. Cao. Carbon monoxide annealed TiO2 nanotube array electrodes for efficient biosensor applications. J. Mater. Chem. 19 (2009) 948–953.

[18] J. Mizera, N. Spiridis, R. Socha, R. Grabowski, K. Samson, J. Korecki, B. Grzybowska, J. Gurul, L. Kepinski, M.A. Malecka. Au/FeOx catalysts of different degree of iron oxide reduction. Catal. Today 187 (2012) 20-29.

[19] W. Temesghen, P.M.A. Sherwood. Analytical utility of valence band X-ray photoelectron spectroscopy of iron and its oxides, with spectral interpretation by cluster and band structure calculations. Anal. Bioanal. Chem. 373 (2002) 601–608.

[20] T. Yamashita, P. Hayes. Analysis of XPS spectra of Fe2+ and Fe3+ ions in oxide materials. Appl. Surf. Sci. 254 (2008) 2441-2449.

[21] R.L. Rebodos, P.J. Vikesland. Effects of oxidation on the magnetization of nanoparticulate magnetite. Langmuir 26 (2010) 16745-16753.

[22] F.J. Beltrán, A. Aguinaco, A. Rey, J.F. García-Araya. Kinetic studies on black light photocatalytic ozonation of diclofenac and sulfamethoxazole in water. Ind. Eng. Chem. Res. 51 (2012) 4533-4544.

[23] F.J. Benitez, J.L. Acero, F.J. Real, G. Roldán. Ozonation of pharmaceutical compounds: Rate constants and elimination in various water matrices. Chemosphere 77 (2009) 53-59.

[24] F.J. Beltrán. Ozone reaction kinetics for water and wastewater systems. Lewis Publ. CRC Press. Boca Ratón, Florida, EEUU (2003).

[25] K. S. Tay, N. A. Rahman, M. R. B. Abas. Ozonation of metoprolol in aqueous solution: ozonation by-products and mechanisms of degradation. Environ. Sci. Pollut. Res. In press. (doi: 10.1007/s11356-012-1223-3).

[26] P.C.C. Faria, J.J.M. Órfão, M.F.R. Pereira. Activated carbon catalytic ozonation of oxamic and oxalic acids. Appl. Catal. B Environ. 79 (2008) 237–243.

[27] J.P. Pocostales, P.M. Álvarez, F.J. Beltrán. Kinetic modeling of powdered activated carbon ozonation of sulfamethoxazole in water. Chem. Eng. J. 164 (2010) 70-76.

[28] B. Kasprzyk-Hordern, M. Ziolek, J. Nawrocki. Catalytic ozonation and methods of enhancing molecular ozone reactions in water treatment. Appl. Catal. B Environ. 46 (2003) 639-669.

[29] J. Nawrocki, B. Kasprzyk-Hordern. The efficiency and mechanisms of catalytic ozonation. Appl. Catal. B Environ. 99 (2010) 27-42.

[30] R. Rosal, A. Rodríguez, M.S. Gonzalo, E. García-Calvo. Catalytic ozonation of naproxen and carbamazepine on titanium dioxide. Appl. Catal. B Environ. 84 (2008) 48-57.

[31] F.J. Beltrán, F.J. Rivas, R. Montero-de-Espinosa. Iron type catalysts for the ozonation of oxalic acid in water. Water Res. 15 (2005) 3553-3564.

[32] H. Taube. Photochemical reactions of ozone in solution. Trans. Faraday Soc. 53 (1957) 656-665.

[33] L. Sánchez, X. Domènech, J. Casado, J. Peral. Solar activated ozonation of phenol and malic acid. Chemosphere 50 (2003) 1085-1093.

[34] E. Mena, A. Rey, B. Acedo, F.J. Beltrán, S. Malato. On ozone-photocatalysis synergism in black-light induced reactions: Oxidizing species production in photocatalytic ozonation versus heterogeneous photocatalysis. Chem. Eng. J. 204-206 (2012) 131-140.

[35] J. Benner, T. A. Ternes. Ozonation of metoprolol: elucidation of oxidation pathways and major oxidation products. Environ. Sci. Technol. 43 (2009) 5472-5480.

[36] F.J. Beltrán, J.P. Pocostales, P.M. Alvarez, J. Jaramillo. Mechanism and kinetic considerations of TOC removal from the powdered activated carbon ozonation of diclofenac aqueous solutions. J. Hazard. Mat. 169 (2009) 532–538.

Table(s)

Table 1. Preparation conditions used for the synthesis of three TiFeC catalysts selected for photocatalytic experiments.

Catalyst sample	FeC magnetic support				TiFeC catalyst	
	AC (g)	Fe (g)	Calcination temperature (ºC)	Calcination time (h)	FeC (g)	Ti (g)
TiFeC-1	10.0	1.1	350	2	3	3.6
TiFeC-2	10.0	4.3	450	3	3	7.2
TiFeC-3	10.0	4.3	550	4	3	7.2

Table 2. Bulk composition (wt.%), XRD crystallite sizes and textural properties of TiFeC catalysts and the activated carbon used as support.

Sample	Fe (%)	TiO_2 (%)	C (%)	d_A (nm)	d_M (nm)	S_{BET} ($m^2 g^{-1}$)	S_{EXT} ($m^2 g^{-1}$)	V_{MICRO} ($cm^3 g^{-1}$)
AC	3.7	0	84.9	---	---	640	51	0.299
TiFeC-1	5.0	53.5	34.3	4.6	9.0	331	65	0.163
TiFeC-2	7.6	65.4	21.2	5.3	16.5	285	113	0.152
TiFeC-3	8.9	64.0	20.0	5.1	17.5	263	118	0.147
TiFeC-3*	n.m.	n.m.	n.m.	5.3	17.9	231	98	0.120

Table 3. XPS results of TiFeC catalysts

Sample	Surface composition (at.%)				Fe 2p peaks position				Ti 2p peaks position	
	Ti (%)	O (%)	C (%)	Fe (%)	Fe $2p_{3/2}$ (eV)	Fe $2p_{1/2}$ (eV)	Sat-Fe^{2+} (eV)	Sat-Fe^{3+} (eV)	Ti $2p_{3/2}$ (eV)	Ti $2p_{1/2}$ (eV)
TiFeC-1	15.2	45.5	37.9	1.4	711.0	724.3	715.3	718.8	459.7	465.4
TiFeC-2	13.0	43.5	41.4	2.1	710.9	724.5	715.4	718.8	459.7	465.4
TiFeC-3	15.0	42.0	39.6	3.4	710.7	724.8	715.4	718.9	459.8	465.5
TiFeC-3*	16.9	45.4	32.6	5.1	712.0	725.1	n.d.	719.3	459.5	465.2

Table 4. Experimental pseudo-first order apparent rate constants (k_{app}) for O_3 depletion in water at different wavelengths

Conditions	k_{app} (min^{-1})	R^2
No radiation	0.071	0.995
390-800nm	0.068	0.995
320-800nm	0.083	0.996
300-800nm	0.123	0.997

Table 5. Pseudo-first order apparent rate constant for MTP depletion in consecutive photocatalytic ozonation runs and iron leached out from catalyst TiFeC-3

RUN	k_{app} (min^{-1})	R^2	Fe_L ($mg\ L^{-1}$)
1	0.040	0.996	0.008
2	0.032	0.997	0.008
3	0.034	0.998	0.006
4	0.037	0.989	0.017
5	0.048	0.990	0.004
6	0.055	0.997	0.014
7	0.036	0.990	0.004
8	0.032	0.993	0.002
9	0.041	0.969	0.008
10	0.048	0.983	0.010

Figure(s)

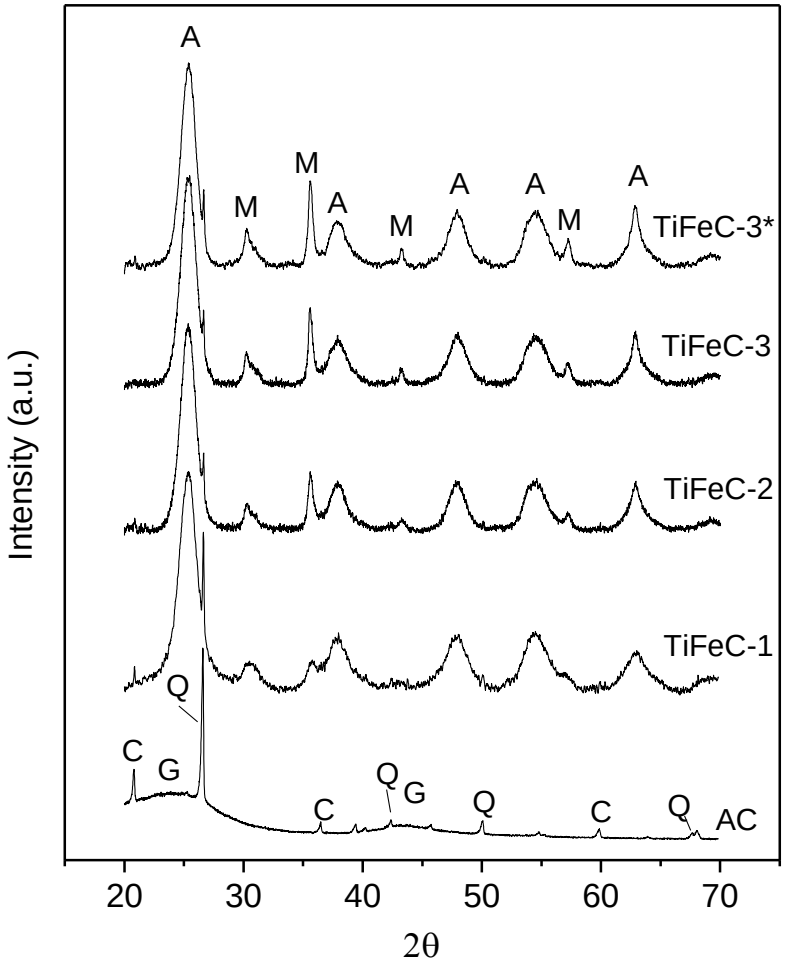

Fig. 1. XRD patterns of the AC support and some TiFeC catalysts. Crystalline phases detected: anatase (A), magnetite/maghemite (M), graphite (G), quartz (Q), cristoballite (C). TiFeC-3* represents catalyst TiFeC-3 after being used in ten consecutive photocatalytic ozonation runs.

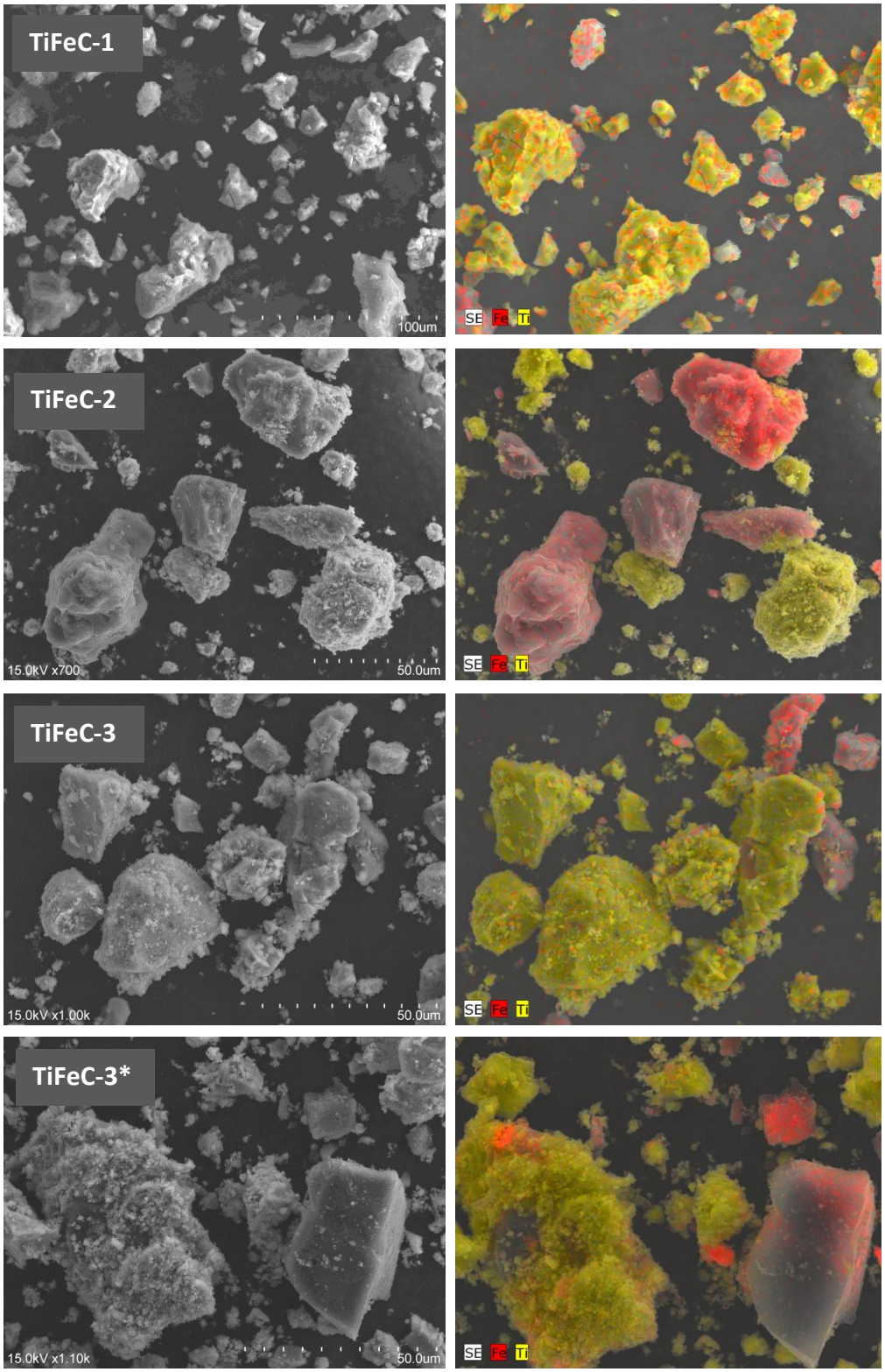

Fig. 2. SEM images (left) and EDX mapping (right) for the TiFeC catalysts

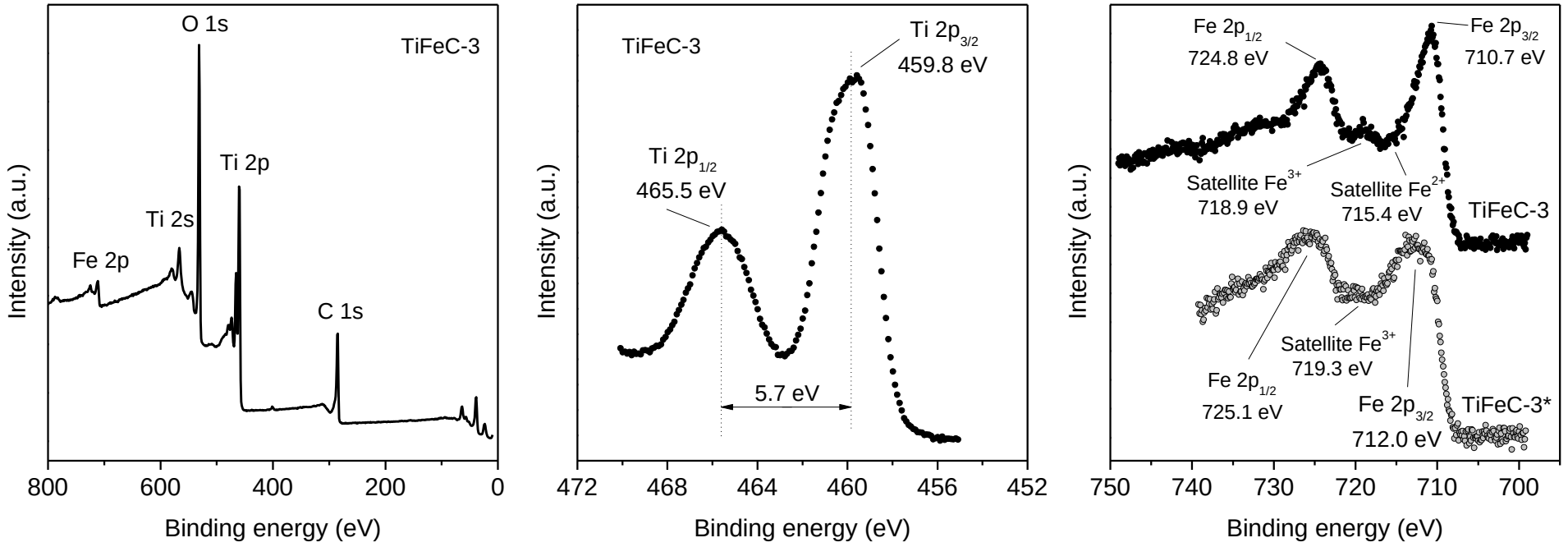

Fig. 3. XPS full spectrum of catalyst TiFeC-3 (a), High-resolution XPS spectra of Ti2p (b) and Fe2p (c) spectral regions

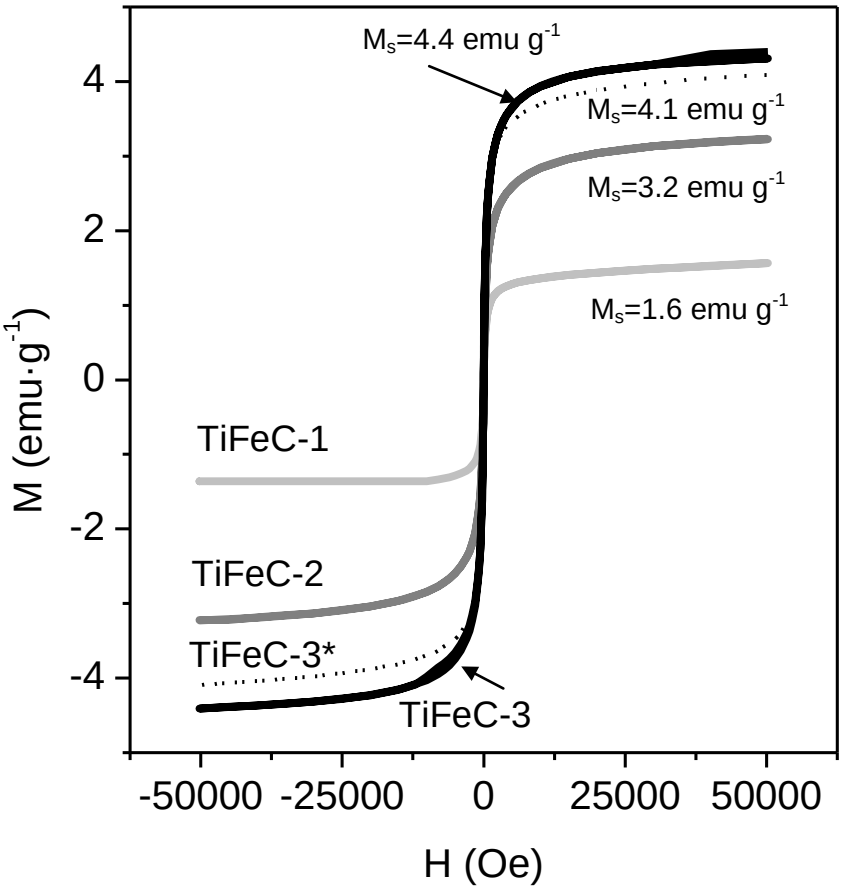

Fig. 4. Magnetization vs. applied magnetic field at 25ºC of TiFeC catalysts

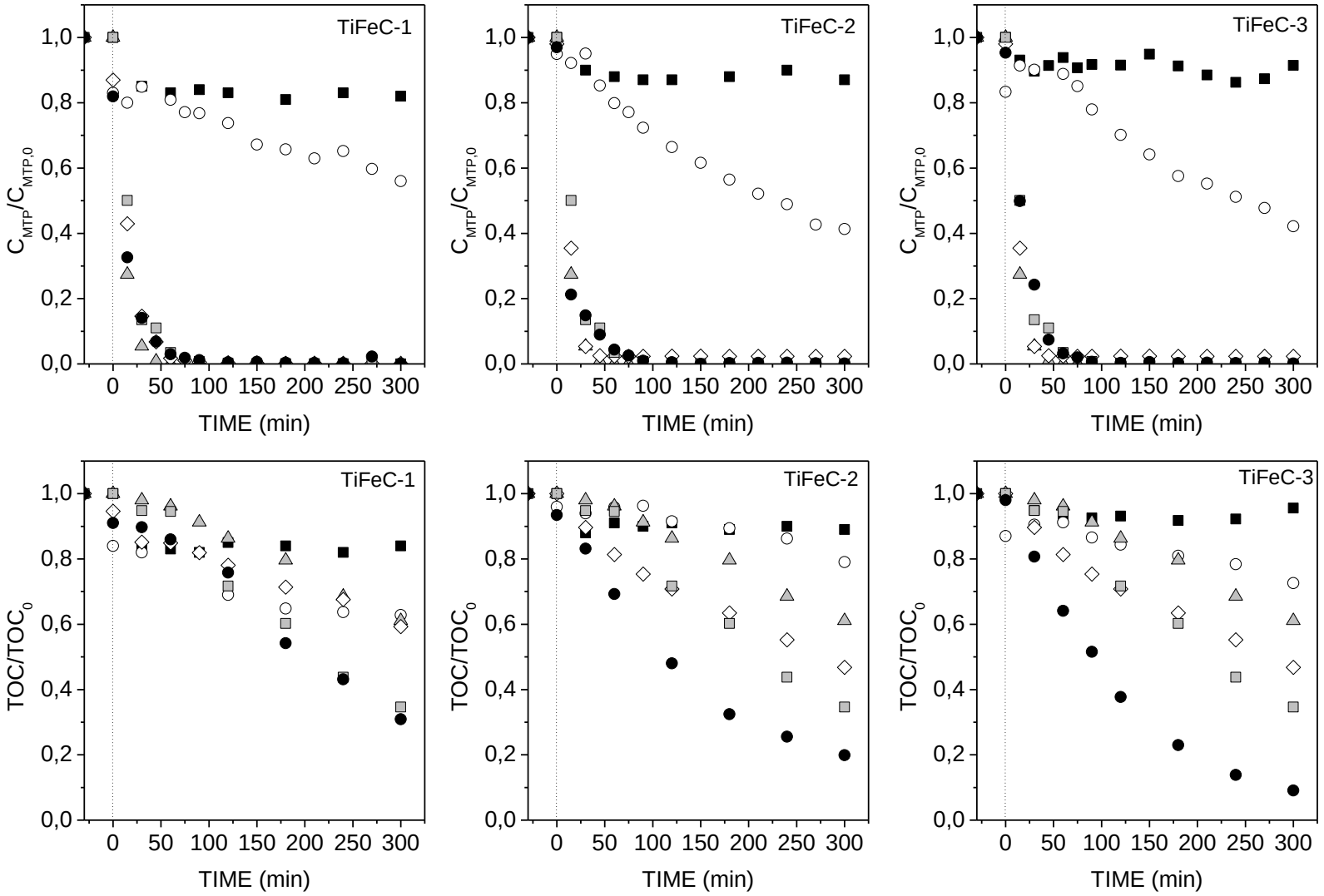

Fig. 5. Evolution of dimensionless MTP concentration and TOC with time. Conditions: C_{MTP_0} = 50 mg L^{-1}, C_{CAT} = 375 mg L^{-1}, gas flow rate = 20 L h^{-1}, $C_{O_3,g}$ = 6 mg L^{-1}. Experiments: adsorption (■), photocatalytic oxidation (○), ozonation (▲), catalytic ozonation (◇), photolytic ozonation(□), photocatalytic ozonation (●)

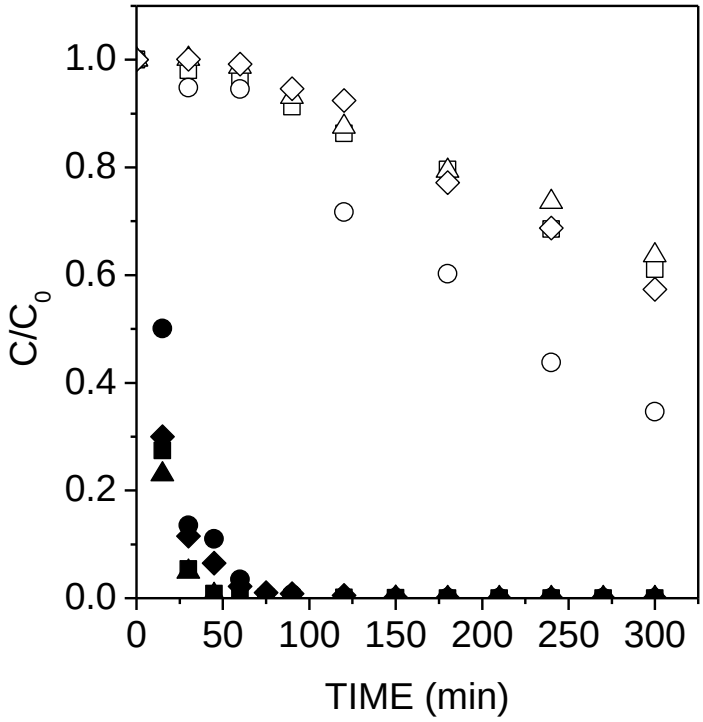

Fig. 6. Evolution of dimensionless MTP concentration (solid symbols) and TOC (open symbols) with time. Conditions: C_{MTP_0} = 50 mg L^{-1}, gas flow rate = 20 L h^{-1}, $C_{O_{3,g}}$ = 6 mg L^{-1}. Experiments: ozonation (■,□), photolytic ozonation (300-800 nm) (●,○), photolytic ozonation (320-800 nm) (▲,△), photolytic ozonation (390-800 nm) (◆,◇)

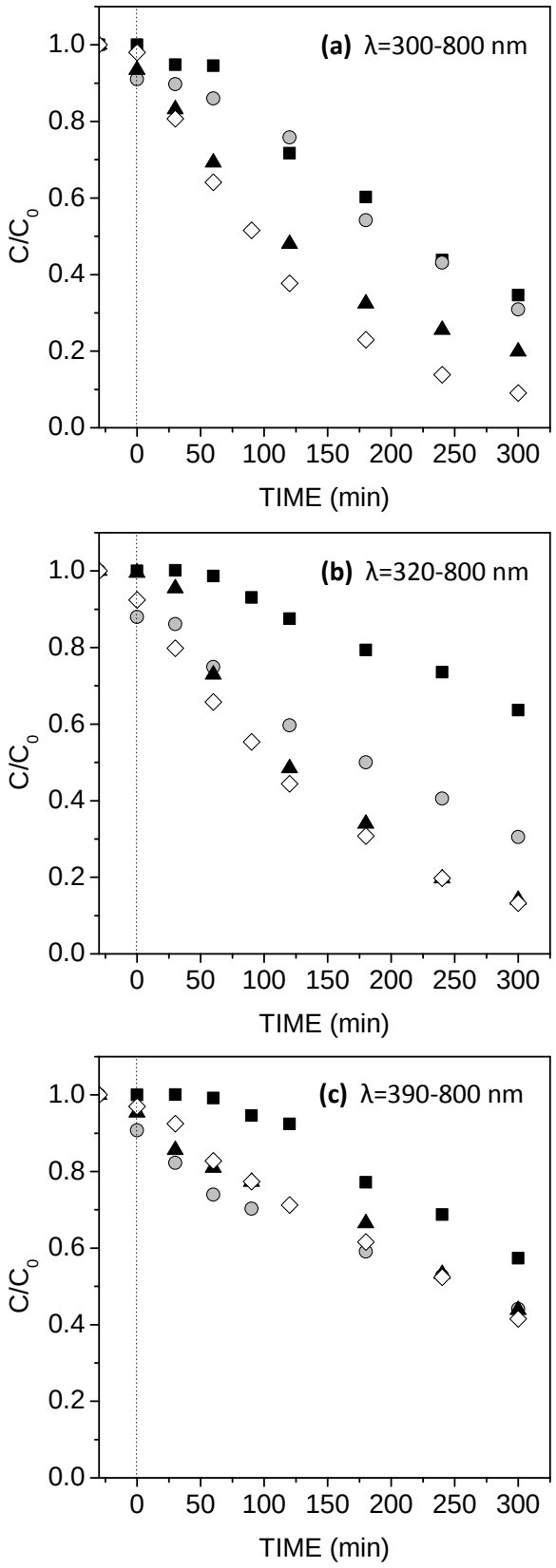

Fig. 7. Evolution of TOC with time. Conditions: C_{MTP_0} = 50 mg L^{-1}, gas flow rate = 20 L h^{-1}, $C_{O_{3,g}}$ = 6 mg L^{-1}. Experiments: photolytic ozonation (■) and photocatalytic ozonation with TiFeC-1 (○), TiFeC-2 (▲), TiFeC-3 (◇)

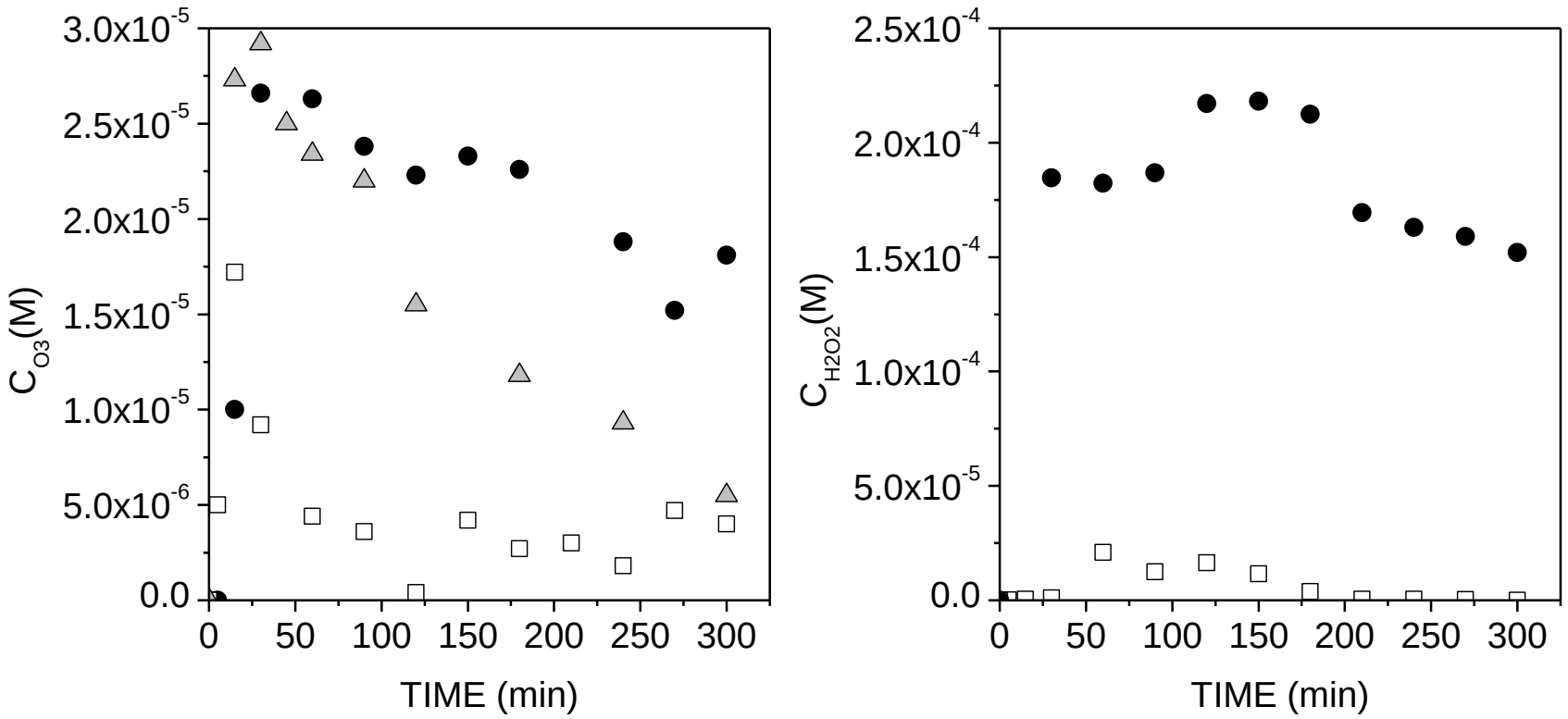

Fig. 8. Evolution of dissolved ozone (left) and hydrogen peroxide (right) with time. Conditions: C_{MTP_0} = 50 mg L^{-1}, gas flow rate = 20 L h^{-1}, $C_{O_3,g}$ = 6 mg L^{-1}. Experiments: Single ozonation (●), catalytic ozonation (△) and photocatalytic ozonation with TiFeC-3 (□)

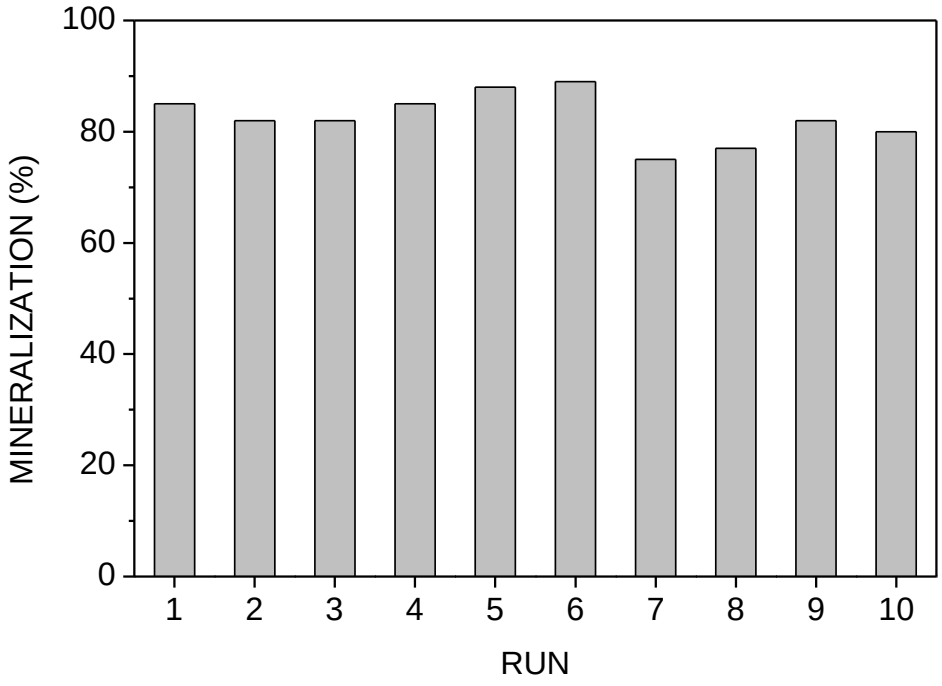

Fig. 9. TOC conversion for consecutive photocatalytic ozonation runs with TiFeC-3 catalyst. Conditions: C_{MTP_0} = 50 mg L^{-1}, C_{CAT} = 375 mg L^{-1}, gas flow rate = 20 L h^{-1}, $C_{O_3,g}$ = 6 mg L^{-1}, radiation wavelength 320-800 nm

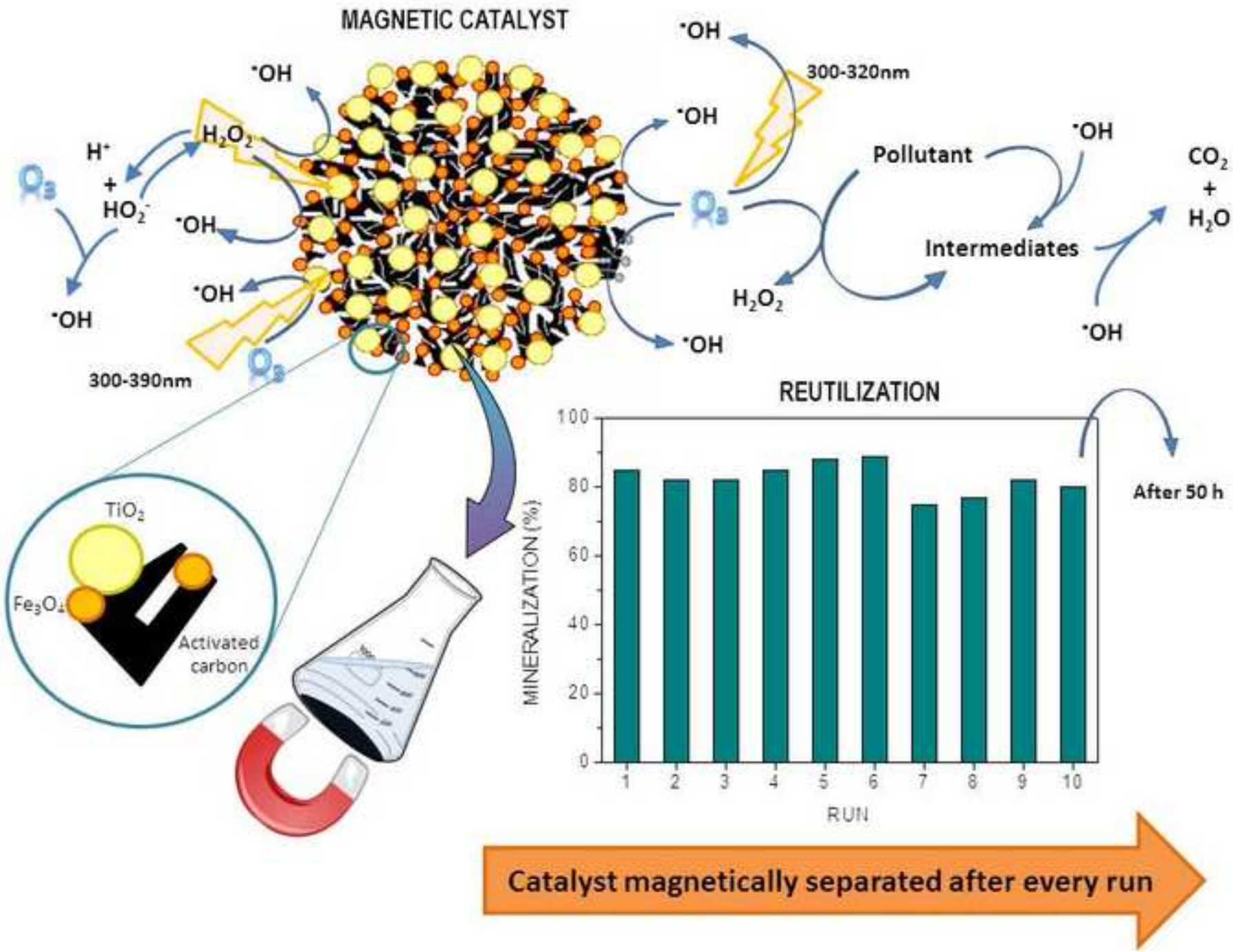
MAGNETIC CATALYST
•OH
•OH
•OH
•OH
•OH
•OH
•OH
300-320nm
H⁺ + HO₂⁻
H₂O₂
O₃
•OH
300-390nm
Pollutant
•OH
Intermediates
CO₂ + H₂O
H₂O₂
•OH
TiO₂
Fe₃O₄
Activated carbon
REUTILIZATION
MINERALIZATION (%)
100
80
60
40
20
0
1
2
3
4
5
6
7
8
9
10
RUN
After 50 h
Catalyst magnetically separated after every run